**Article:**
Ali, SA and Forth, JP (2021) An experimental and analytical investigation of reinforced concrete beam-column joints strengthened with a range of CFRP schemes applied only to the beam. Advances in Structural Engineering, 24 (12). ARTN 13694332211007371. pp. 2748-2766. ISSN 1369-4332

https://doi.org/10.1177/13694332211007371

## Abstract

This paper investigates the experimental and analytical behaviour of beam-column joints that are subjected to a combination of torque, flexural and direct shear forces, where different Carbon Fibre Polymer (CFRP) strengthening wraps have been applied only to the beam. These wrapping schemes have previously been determined by the research community as an effective method of enhancing the torsional capacities of simply supported reinforced concrete beams. In this investigation, four ¾-scale exterior beam-column joints were subjected to combined monotonic loading; three different beam wrapping schemes were employed to strengthen the beam region of the joint. The paper suggests a series of rational formulae, based on the space truss mechanism, which can be used to evaluate the joint shear demand of the beams wrapped in these various ways. Further, an iterative model, based on the average stress-strain method, has been introduced to predict joint strength. The proposed analytical approaches show good agreement with the experimental results. The experimental outcomes along with the adopted analytical methods reflect the consistent influence of the wrapping ratio, the interaction between the combined forces, the concrete strut capacity and the fibre orientation on the joint forces, the failure mode and the distortion levels. A large rise in the strut force resulting from shear stresses generated from this combination of forces is demonstrated and leads to a sudden-brittle failure. Likewise, increases in the beams' main steel rebar strains are identified at the column face, again influenced by the load interactions and the wrapping systems used.

## 1 Introduction

The role of the beam-column joint is crucial in providing an efficient load path between the beam and column elements. Poorly detailed or inadequately designed reinforced concrete (RC) beam-column joints lead to excessive deformations and an increase in columns loads; ultimately, this may affect the stability of the structure. Thus, a large number of tests have been carried out to investigate the behaviour of RC beam-column joints under monotonic or cyclic loading; generally, these tests involved the concentric loading of the beams and columns, i.e., Mostofinejad and Hajrasouliha (2019); Mostofinejad et al. (2018); Davood and Alireza (2017); Sasmal (2009), Triantafillou and Antonopoulos (2003); Hamil (2000); Parker (1997); Sarsam and Phipps (1985). However, in practice, structural members undergo a combination of both concentric and eccentric (torsion) loads during the construction stages and their working life. Torsional forces can result from alternating span loadings and direct eccentric loads, which can promote severe cracks in RC beams, especially in exterior frame joints. The presence of torsional forces reduces the shear and flexural capacity of RC members (Peng and Wong, 2011). Moreover, torsional forces increase the tensile stresses of the steel bars and effectively alter the plastic hinge locations (Ali and Forth, 2018). Since 2001, a number of torsional strengthening and upgrading schemes for RC beam members involving Fibre Reinforced Polymers (FRP) composites have been presented (Table 1). The use of FRP in this way is largely due to the simplicity of its installation and the superior physical characteristics of FRP over conventional retrofitting materials, such as steel and concrete.

In comparison to concentrically loaded joints, there has been much less research into the effect of beam torsion on joint behaviour. Research has concentrated on the influence of the eccentricity of the beam axis on the column axis (Kusuhara et al., 2004; SHIMIZU et al., 2000; Raffaelle et al., 1992), as well as the effect of transverse beams and slabs (Hassan, 2011). More recently, Elshafiey et al. (2016) did investigate the effect of beam torsional moments on beam-column joints. They found that the observed failures occurred in the joint regions due to a lack of joint stirrups and high beam stiffness.

Interestingly, the FIB Model Code (Fédération Internationale du Béton) (2010) and Eurocode 2 (2004) propose at the ultimate limit state that it is not necessary to consider torsion induced loading (by compatibility); to avoid excessive cracking, minimum reinforcement should be incorporated by way of stirrups and longitudinal bars (FIB Model Code (Fédération Internationale du Béton), 2010). Similar guidance is also provided in the ACI Committee 318 (2014) for forces

within the threshold limit (the threshold limit is defined as 25% of the torsional cracking moment). In summary, the general recommended design provisions for RC joints (ACI-ASCE 352R-02 Committee, 2002; Eurocode 2, 2004; NZS 3101, 2006; BS8110, 1997) do not provide guidelines to evaluate joint shear demand under combined actions, including torsion.

This paper investigates the influence of beam torque on equivalent exterior frame beam-column joints strengthened with various CFRP wrapping scheme. The paper proposes an analytical model that allows the prediction of joint forces and hence, capacities. In doing so, it presents the development of a number of formulae that can be used to evaluate the forces in the main tension ties and compression struts under the combined action of torsional, flexural and direct shear forces, depending on the different wrapping schemes.

## 2 Beam torsional strengthening schemes.

A summary of the available research that has experimentally investigated externally bonded FRP systems for beams is presented in Table 1. It has been found that various improvements in beam torsional capacity could be achieved by using different wrapping systems. Based on the fibre orientation and the section wrapping system, the beam test configurations can be categorised into five main schemes - continuous vertically oriented wraps along the beam member; U-wrap; strip wrap (hoops); 45$^{o}$ oriented fibres; and horizontally oriented wraps. The vertically and 45$^{o}$ oriented carbon fibre arrangements attained the highest loading levels (Ghobarah et al., 2002; Panchacharam and Belarbi, 2002; Chalioris, 2008; Deifalla et al., 2013; Salom et al., 2004), whereas the partially wrapped arrangement (U-wrap) was less effective than the fully wrapping schemes and exhibited premature de-bonding. The influence of horizontally oriented fibres on beam torsional strength appeared to be insignificant (Zhang et al., 2001; Patel et al., 2016).

Although, several beam configurations using glass fibre reinforced polymers (GFRP) have been researched, typically they exhibited a drop-in enhancement level compared with the CFRP wraps (Ameli et al., 2007). As the effect of beam wrappings on joint integrity and stress variations have not been identified yet, this research investigates the influence of beam wrapping systems on stress levels in the tension chords and compression struts of beam-column joints, paying particular attention also to joint deformation and failure regions. Further, this study presents a rational approach to quantifying the increase in the stresses within the beam main rebars which transfer to the joint area as influenced by the proposed beam wrapping schemes. These wrapping schemes can

potentially increase the beams' capacities, stiffness, and levels of plastic deformations to a sufficient level such that damage occurs in the column of the joint, negating the preferable strong column – weak beam behaviour. Hence, it is important to develop this rational approach such that the effects of the wrapping schemes (and any changes to the combined forces resulting from a change in building use or a structural change to the frame) can be accurately quantified; ultimately ensuring that the damage is kept away from the joint and is located in the beam itself.

## 3 Experimental Programme

### 3.1 Specimen details

Four ¾-scale exterior beam-column joints (SH-C-U, SH-S-C-A, SH-S-C-H, and SH-S-C-I) were constructed using normal weight concrete and high strength steel bars. The specimens' details are given in Table 2 and the member sections and dimensions are shown in Figure 1-a. The beam and column lengths of the exterior joint have been extended beyond the contra-flexure points (analytically determined as part of a hypothetical six-storey ordinary moment resisting frame). The members were designed according to the ACI Committee 318 (2014) recommendations, while the joint panel details satisfy the ACI-ASCE 352R-02 Committee (2002) recommendations - connection Type-1. Hooked end bars (90$^o$) were used without any splice to provide a sufficient bonding length and to prevent anchorage failure in the joint's horizontal bars. The joint's aspect ratio is 1.05; it was noted that a number of previous studies have noted a decrease in joint shear capacity with an aspect ratio larger than 1.4 (Chun and Shin, 2014; Hamil, 2000). As part of the analysis of the hypothetical 6-storey frame, a non-symmetrical distribution of live loads was considered between the floors and spans, such that the maximum induced beam torque did not exceed the threshold limit specified by ACI Committee 318 (2014). In the beam region, no additional torsional reinforcement was therefore provided.

### 3.2 Material properties

The ultimate strengths of the steel bars are 560 MPa, 540 MPa and 570 MPa for the Φ16mm, Φ12mm, and Φ8 mm, respectively. Three bars of each diameter were selected and uniaxial tensile tests were performed to determine the tensile strength. The average compressive results for concrete samples are given in Table 2, where the samples were tested at 28 days. Three effective CFRP wrapping schemes (full wrapping, hoops, and 45$^o$ wraps) were employed to strengthen the

SH-S-C-A, SH-S-C-H and SH-S-C-I specimens, as shown in Figure 1-b. Enhancements to the torsional strength of each joint specimen were evaluated in accordance with the FIB Bulletin 14 (2001) provisions. Surface preparation and corner rounding were performed before the sheets were applied to the concrete substrate. The coupon details of an un-impregnated unidirectional CFRP fabric are as follows: (1) tensile strength =2530 MPa, (2) tensile modulus =230 GPa, ultimate tensile strain= 1.5%, and thickness = 0.22 mm. A medium viscosity resin (epoxy) was used to attach and impregnate the CFRP fabrics.

### 3.3 Test setup and instrumentations

All tests were conducted under monotonic loading. A rigid steel arm was attached to the end of the beam furthest from the column. The steel arm was orthogonal to the span of the beam (see Figure 1-c) and allowed the monotonic point load to be applied via hydraulic jack at a distance of 1.57m from the vertical centreline of the beam (the torque arm); this produced torque, in addition to bending and vertical shear. A constant compressive axial load of a pre-specified magnitude ($0.1\ A_g\ fc'$) was applied to the column ends during the tests which represents a typical load from the upper floors of a structure as recommended by the design codes (ACI Committee 318, 2014; Eurocode 1, 2002). The influence of the column's axial load on the ultimate joint strength is still being debated in the extant literature. However, the improvement of the joints capacities was observed for the tested joints that subjected to low and medium axial load ratio ranging from 0.1 to 0.3 of the column load capacity (Shannag and Alhassan, 2005; Parvin et al., 2010). Further, Antonopoulos and Triantafillou (2003) observed a rise in the joint shear strength for externally wrapped beam-column joints by increasing the column axial load to $0.1\ A_g\ fc'$. In contrast, a high level of axial load could induce buckling of column's rebars or promoting sudden joint's failures (Shigeru Hakuto and Hitoshi, 2000).

Several Linear Variable Differential Transducers (LVDT's) were employed to measure the twist angle (LVDT 3 to 6) and joint deformations (LVDT 1 & 2), as illustrated in Figure 1-c. Also, a number of strain gauges were mounted on the steel bars of size 5mm and size 2mm on the CFRP sheets to capture the strain development through all loading stages.

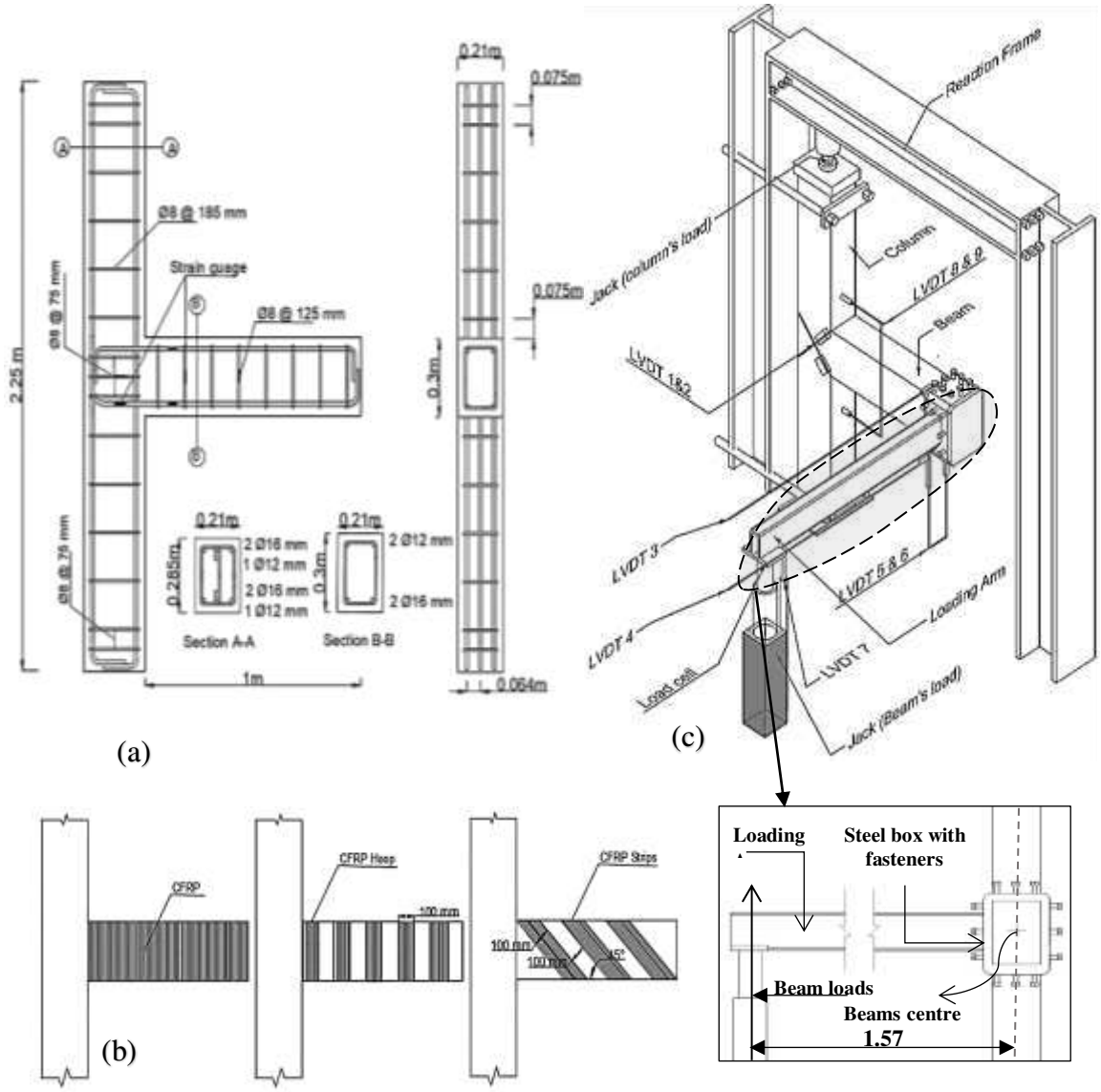


**Figure 1.** (a) Specimen details (b) Scheme details (c) Test Set-up

## 4 Experimental results and discussion

The behaviour of the joint specimens is quantified in Figure 2. From Figure 2 it can be seen that the loading capacity increases proportionally with an increase in the wrapping ratio ($\rho_f$); the fully wrapped specimen (SH-S-C-A) has attained the maximum loading levels (Figure 2 a, b, and c). First cracking was observed in the beams; progressive inclined cracks developed around the beams and along their lengths. Several cracks propagated into the joint zone of the SH-S-C-A and SH-S-C-I (Figure 3-a and 3-b) due to the increase in shear demand resulting from the torsional forces. Evidence of this increase in shear demand was observed in the strains measured in the beam's

main bars (Figure 6-b); these measurements were taken 100 mm away from the column face. This behaviour also influenced the joint deformation angle ($\gamma$), as shown in Figure 2-f. The evaluation method for the shear distortion angle is schematically illustrated in Figure 4-a.

Failure of the specimens mainly occurred in the beam regions and was due to the crushing of the concrete struts. In comparison with the unstrengthened specimen (SH-U-C), the fully wrapped specimen (SH-S-C-A) exhibited beam damage which extended to the column face. The beam's damage (SH-S-C-A) was concentrated in a region under relatively high bending moment near the column face, where the flexural compressive forces intensified the concrete strut forces that were induced by both the torsion and shear actions. Hence, when subject to torsion, it is crucial to improve the strength of the concrete strut in order to avoid catastrophic brittle failure. The compressive strength of the diagonal struts is greatly influenced by the softening of concrete (the cracking stage), which was enhanced due to the increase in orthogonal tensile stresses caused by shear stresses.

It was clear that by using CFRP hoops (SH-S-C-H) the cracking levels were reduced as compared with the control specimen (SH-U-C); see Figure 5-a and Figure 5-b. The CFRP hoops tend to reduce the cracking levels (e.g. during both the ascending and descending stages) and tend to improve the concrete response, i.e. by (1) increasing the confinement of the concrete through the lateral pressure provided by the CFRP hoops, and (2) resisting the diagonal tensile stresses. Although the SH-S-C-I specimen experienced relatively lower concrete deformations and fewer cracks than the SH-S-C-H specimen after the cracking load was reached, sudden damage occurred in the concrete struts when the induced forces in the inclined compressive struts exceeded the softened concrete's compressive strength, which impaired the member's ductility.

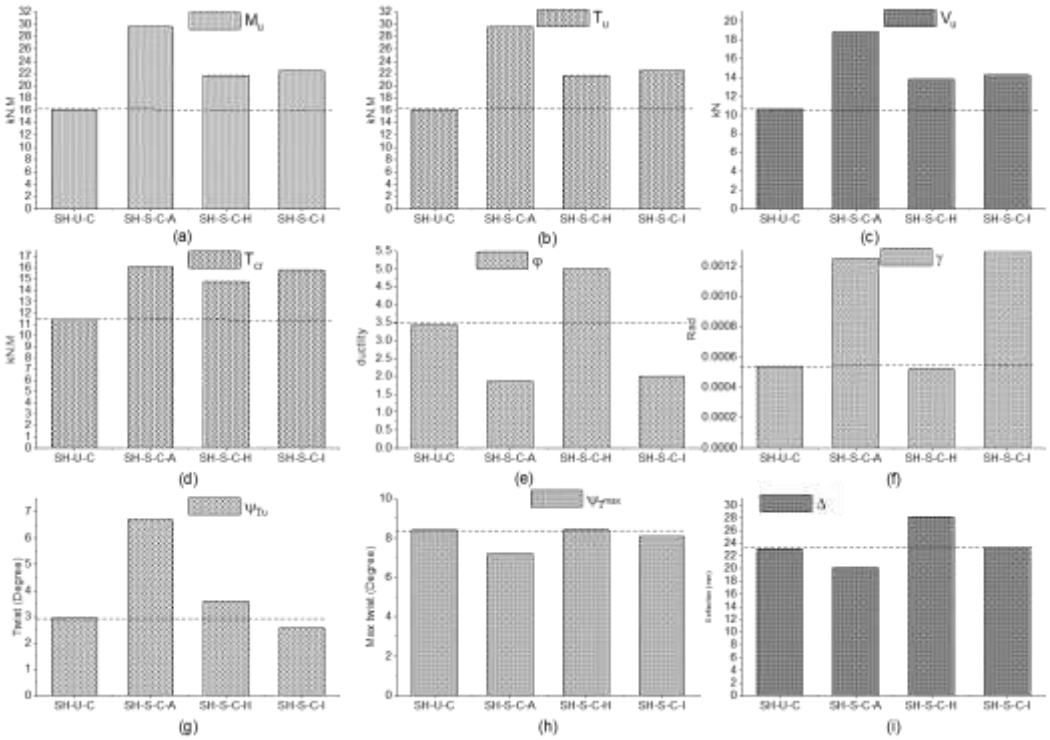


**Figure 2.** Tests results: (a) Ultimate bending moment, (b) Ultimate Torque, (c) Ultimate vertical shear, (d) Cracking Torque, (e) Ductility index, (f) Shear distortion angle, (g) Twist angle at $T_u$, (h) Max twist angle, (i) Max. Beam deflection.

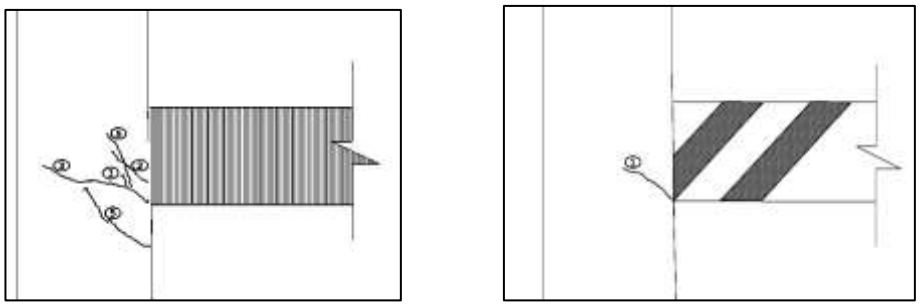


**Figure 3.** Joint cracks (a) Fully wrapped specimen (SH-S-C-A) (b) 45º degree wrapped specimen (SH-S-C-I)

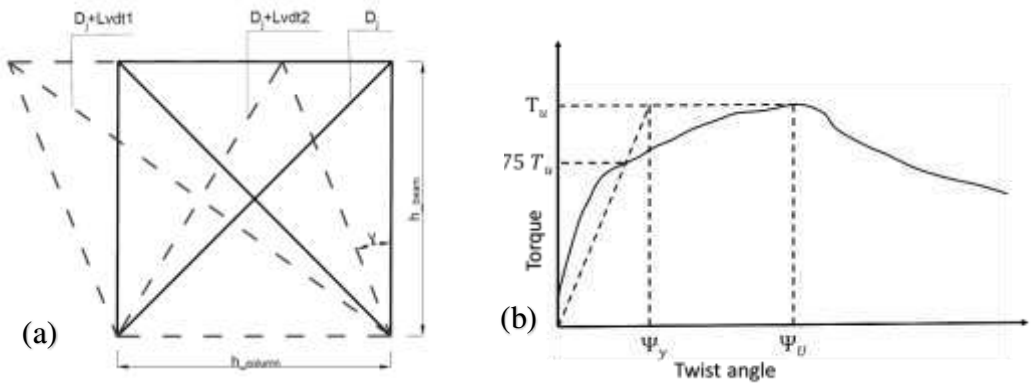


**Figure 4.** Schematic diagrams: (a) joint shear distortion angle, (b) ductility level, yield displacement of the reduced stiffness equivalent elasto-plastic system.

(a) (b)

**Figure 5.** Beam cracks: (a) SH-U-C specimen, and (b) SH-S-C-H specimen

### 4.1 Load-Twist Behaviour

During the first stages of loading, the behaviour of all tested specimens was very similar (Figure 6-a) - this linear elastic behaviour continued with high torque-twist ($T_{cr}$- $\psi_{cr}$) rigidity up to the cracking load. As mentioned earlier, the strengthened specimens demonstrated different levels of enhancements to their cracking strength, although all exceeded the cracking strength of the unstrengthened specimen (SH-U-C).

These enhancements reflect the degree of confinement of the CFRP wraps and the fact that the CFRP wraps delay the cracks in the concrete by reducing the orthogonal tensile stresses. The strengthened specimens demonstrated a progressive increase in their load carrying capacities in the post cracking stage (ascending curves). Moreover, the strengthened specimens produced a larger torsional rigidity than the control specimen (SH-U-C), with both the SH-S-C-I and SH-S-C-A exhibiting a linear response up until the maximum load was reached. The SH-U-C-H specimen, on the other hand, exhibited a non-linear behaviour up to the maximum load this was as a result of the propagation of the beam's concrete cracks starting immediately after the cracking load in the regions between the CFRP hoops. Further, there was yielding of the steel stirrups prior to the ultimate load.

The last stage (failure stage) for specimens SH-S-C-I and SH-S-C-H was identified following the loss of the member's carrying capacity after the peak load was reached. At this stage, significant deterioration in the member's torsional stiffness was observed due to severe concrete cracks, large plastic deformations in the steel stirrups and rupture of the CFRP strips. For the fully wrapped specimen SH-S-C-A, the declined failure stage did not develop due to brittle concrete failure, followed by the fracturing of the CFRP wraps shortly after the peak load.

Table 3 compares the strengthened specimens with the unstrengthened specimen in terms of cracking torque ($\Delta T_{cr}$), ultimate torque ($\Delta T_u$), torsional cracking rigidity ($\Delta K_{cr}$), and post-cracking rigidity ($\Delta K_u$), and illustrates the percentage increase in performance offered by the CFRP wrapping.

The specimens' torsional rigidities ($K_{cr}$ and $K_u$) were evaluated as the measured torque with respect to the unit angle of twist at the cracking and ultimate load, respectively. It can be concluded from Table 3 that the effectiveness of the CFRP wraps in increasing the member's torsional rigidities is significantly pronounced during the post-cracking stage. These increases in post-cracking rigidities ($\Delta K_u$) ranged from between 35% for the CFRP strip schemes and 114% for full continuous wraps. In contrast, the influence of these external wrapping schemes before cracking ($\Delta K_{cr}$) was not very significant.

### 4.2 Ductility Levels

The ductility index has been evaluated as the ratio of rotation ($\psi_u$) at the peak load and the yielding point, as schematically illustrated in Figure 4-b. An equivalent elastic-plastic system was employed to identify the equivalent yielding point for the specimens, as they exhibited different levels of cracking and yielding through the loading stages, along with the yield displacement of the reduced stiffness, an equivalent elastic-plastic system was employed. This system was suggested by Park (1988).

Figure 2-e shows the ductility index for all beam-column joints; it can be noticed that the member's ductility in terms of torque-twist (T-$\psi$) has reduced in accordance with the level of torsional forces attained. As a result of incorporating beam torsion, the failure of the specimens mainly occurred in the beam regions and was attributed to progressive degradation in the concrete's strength (as observed for SH-U-C and SH-S-C-H), or sudden crushing of the concrete struts with the complete rupture of the CFRP sheet (as observed in the failure of SH-S-C-A), both significantly reduced the ductility level. The T-$\psi$ ductility indices demonstrate that the specimens were considerably affected by the degree of wrapping, with the highest level of ductility being achieved when CFRP hoops were used. However, the brittle failure of the fully wrapped specimen illustrates the need for a balance between the enhancement level due to the wrapping schemes and the concrete strut's capacity. Further, the ductility levels for all specimens can be adversely affected if the specimens exhibit joint shear failures, anchorage failure, or slippage of the beam tension rebars within the joint region. Therefore, the increase in the joint's demands due to both combined forces

and wrapping schemes should be quantified, with a view to avoid brittle shear failures in the joint zones.

### 4.3 Strain Developments

A decrease in the member loads occurred once the steel rebars yielded. There was also a severe deterioration in the stiffness of the beam after the rupture of the CFRP wraps and when yielding of the steel stirrups had occurred. Figure 6-b and Figure 6-c show that a higher tensile strain developed in the bottom steel (flexural tension zone) of the beam (yielded) than in the top steel, due to the fact that the torsional and bending forces were additive. Based on the truss mechanism, the increase in strain in the transverse reinforcement increased the angle of the inclined struts such that they became steeper and reduced the amount of stress in the longitudinal main rebars. This is reflected in the behaviour of the SH-S-C-H and SH-C-S-A specimens, where under the same load levels they produced lower strain values than the unstrengthened control specimen (SH-C-U). For the SH-S-C-I, the inclined wraps tended to reduce the concrete strut angle and produce larger longitudinal strains (plastic deformations). In the middle of the column zone, the levels of developed strains in the beam's bottom rebars had decreased due to the forces in the steel being transmitted by bond into the concrete within the joint zones (Figure 6-d). However, the joint steel ties of all the specimens exhibited insignificant strain rates (less than 130 micro-strain), as a tie strain emerges under high joint shear forces near the failure load (Hamil, 2000).

Figure 7-a and Figure 7-b show the strain development in the CFRP sheet and steel stirrups at a distance of 250 mm away from the joint zone. These figures reveal that significant strains occurred in the CFRP sheets and beam steel stirrups due to the shear stresses. The CFRP wraps were highly strained in the regions close to the failure zones (see SH-S-C-I and SH-S-C-A specimens). The inclined CFRP configuration (SH-S-C-I) exhibited early strain development, which was consistent with the main rebar's deformations, as mentioned earlier. A good agreement can be observed between the maximum observed strain levels and the evaluated effective strain ($\varepsilon_{ef}$), according to Eq. 5.2i, which utilises the level of tensile strain in the concrete substrate in its prediction (Figure 7a).

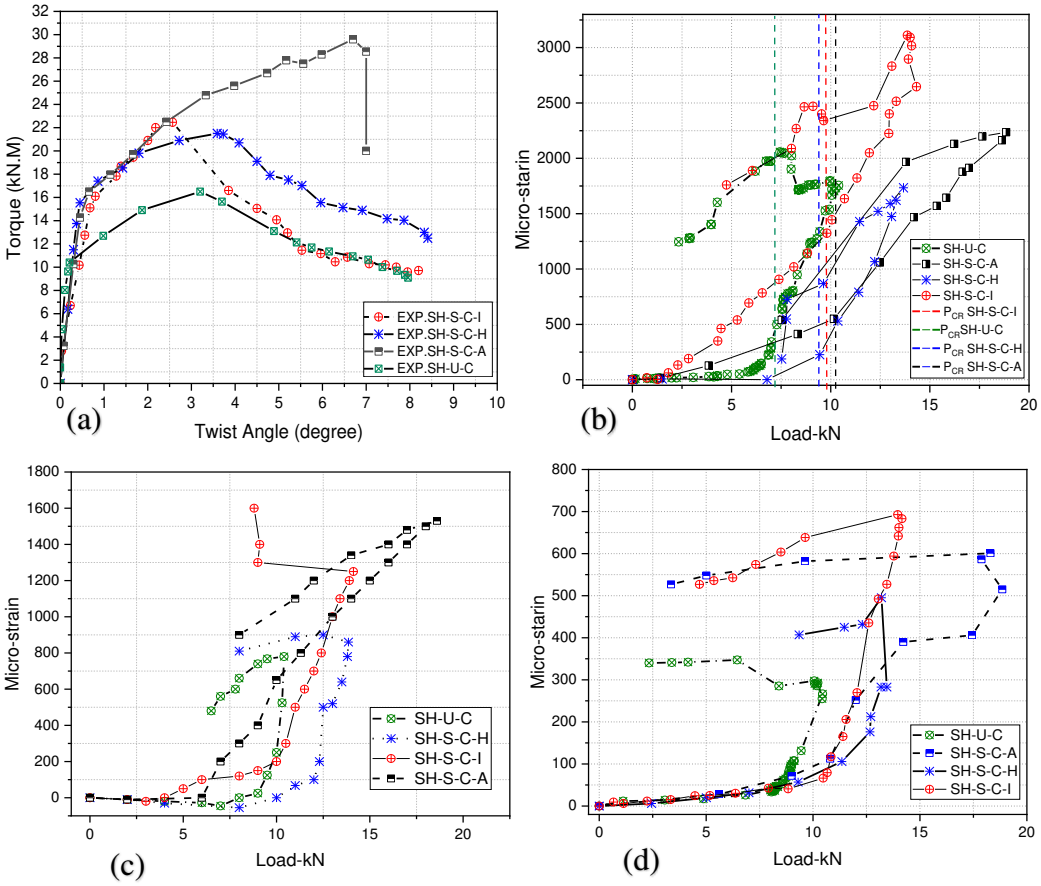


**Figure 6.** (a) Torque-twist angle diagram, (b) Steel strain of the bottom main bars near the column face, (c) Steel strain of the top beam main bars near the column face, (d) Steel strain of the main bars in the middle of the joints.

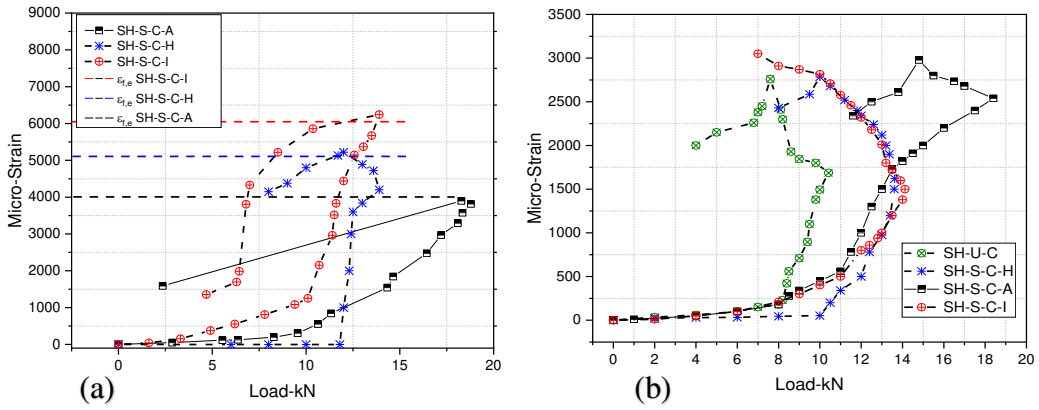


**Figure 7.** (a) CFRP strain at 250 mm from column face, (c) Beam stirrup strain.

## 5 Concrete strut capacity and shear demand

The occurrence of torsion with other forces, such as flexure and vertical shear, is quite common. This combination of forces produces a variation of strain around the perimeter of the cross-section and over the member's length. The test results of this investigation conform with the space truss analogy, as the combination of flexural and shear stresses magnified the tension forces in the beam's main rebars, along with the compression forces in the concrete struts. In this context, during

the post-cracking stage, the space truss model is formed from the longitudinal and transverse ties and the concrete struts. Thus, to diminish the crushing of concrete resulting from the interaction between the direct shear and torque, this study attempts to limit the torsional enhancement levels (via the CFRP) to the concrete strut capacity ($\sigma_d$). These enhancement levels can be predicted using FIB Bulletin 14 (2001) (Eq. 5-1), which has been developed according to the space truss mechanism, and suggests that the design concrete inclination angle ($\alpha_d$) is equal to 45°. The test results indicate that a better correlation between predicted and actual $Tu_{frp}$ can be achieved by utilising the effective ($\varepsilon_{ef}$) FRP strain (Eq.5-2i and Eq.5-2ii). The $\varepsilon_{ef}$ is based on the work by Triantafillou and Antonopoulos (2000) and the calibration of the published experimental data, which correlates $\varepsilon_{fe}$ with the concrete tensile strength of concrete. This was modified according to the effective fibre ratio (Eq.5-3) and the thin-walled analogy, as developed by Hii and Al-Mahaidi (2007). The thin-walled truss mechanism is recommended by the major codes of practice, including ACI Committee 318 (2014) and Eurocode 2 (2004), to evaluate torsional member capacity, since it includes the steel rebar contribution ($Tu_{steel}$). The overall expected torque should be computed by the superposition of the contributions from the steel rebars and the CFRP.

The reduction in concrete strut capacity-vertical component ($\sigma_{d_v}$) can be evaluated according to Eurocode 2, as given in Eq.5-4. This is also stipulated by CEB-FIP (1991) for concrete that is essentially under compression stresses. The maximum strength ($f_{d_v}$) attained by the inclined concrete strut in the transverse direction can be evaluated according to the truss method (Eq.5-5), as the angle of inclination ($\alpha_d$) can either be assumed as per Eurocode 2 (2004) or calculated directly using Eq.5-8 to 5-11, 5-13 and 5-15 (these will be discussed later). Figure 8-a illustrates the truss mechanism at the member side, where the maximum shear flow ($q_i$) resulted from the addition of torque and vertical shear ($V_u$). This investigation identified that wrapping schemes can enhance the confinement degree and reduce the softening of concrete from tensile cracking. This study recommends Eq.5-4 for both strengthened and unstrengthened members to conservatively avoid any failure in the concrete. However, for a favourable redistribution of shear stresses over the member's depth, a root-square summation of direct shear and torsional forces has been applied to verify the member's capacity (Eq.5-6). This agrees with the recommendations of ACI Committee 318 (2014) for solid sections, while 85% of the section's area that is enclosed by stirrups ($A_o$) is utilised to evaluate the shear flow area resulting from the torque actions (Figure 8-c).

$$T_{Ufrp} = 2\,\varepsilon_{ef}\,E_f\frac{t_f\,b_f}{S_{sf}}\,A_o\,(\cot(\alpha_d)+\cot(\alpha_f))\sin(\alpha_f)\,10^3 \quad (5\text{-}1)$$

$$\varepsilon_{ef} = 0.17\left(\frac{f_c'^{\frac{2}{3}}}{E_f\,\rho_f}\right)^{0.3} k\,\varepsilon_{fu} \le \varepsilon_{max} \quad \text{[ Full CFRP wraps]} \quad (5\text{-}2i)$$

$$\varepsilon_{ef} = 0.65\left(\frac{f_c'^{\frac{2}{3}}}{E_f\,\rho_f}\right)k^{0.3}\times 10^{-3} \le \varepsilon_{max} \quad \text{[Debonding failure (U or partial CFRP warps)]} \quad (5\text{-}2ii)$$

$$\rho_f = \frac{4t_f\,b_f\,U_c}{3A_g\,S_{sf}} \quad (5\text{-}3)$$

$$\sigma_{d_v} = 0.6\left(1-\frac{f_c'}{250}\right)f_{d_v} \quad (5\text{-}4)$$

$$f_{d_v} = \frac{f_c'}{(\cot(\alpha_d)+\tan(\alpha_d))} \quad (5\text{-}5)$$

$$\sqrt[2]{(V_u)^2+\left(\frac{(Tu_{frp}+Tu_{steel})U_c}{0.85(2A_o)}\right)^2}\,(A_*)^{-1} \le \sigma_{d_v} \quad (5\text{-}6)$$

Where $f_c'$ is the concrete compressive strength in MPa; $E_f$ is the FRP Young's modulus in GPa; $\rho_f$ is the effective FRP ratio; $\varepsilon_{fu}$ is the FRP ultimate strain; $t_f$ is the FRP thickness in mm; $\varepsilon_{max}$ = 0.005 ; K is the FRP strain reduction factor ($K = 0.8$); $b_f$ is the FRP strips width in mm; $U_c$ is the outer perimeter of the section in mm; $A_g$ is the section's gross area in mm$^2$; $S_{sf}$ is the spacing between the FRP strips c/c in mm; $\alpha_f$ is the orientation of fibres measured form the beam longitudinal axis in degrees; $d_v$ is the effective depth between the top and bottom rebars between top and bottom rebars (d-d`) in mm; $b_v$ is the effective width of the beam in mm ; $A_*$ is the area that is equivalent to $A_g$ for strengthened sections in mm$^2$, or the equivalent to a magnitude of ($A_o$) for unstrengthened sections.

The joint shear demand (joint forces) resulting from the combination of the beam forces can be quantified according to the truss mechanism. The interaction between torsion, bending and direct shear according to the space truss analogy was reported by Elfgren (1972) and later by Rabbat and Collins (1978), and Hsu (1996). This present study has extended this method to evaluate the tensile forces in the main rebars in the flexural tension zone of the beam, by considering the effect of the various CFRP wrapping schemes and subsequently establishing the relevant formulae that conform to the truss method. Eq. 5-7 satisfies the equilibrium of forces by taking a moment about the top chords (Figure 8-b) - the bottom beam's side being exposed to tensile stresses induced by the flexural and torsional forces.

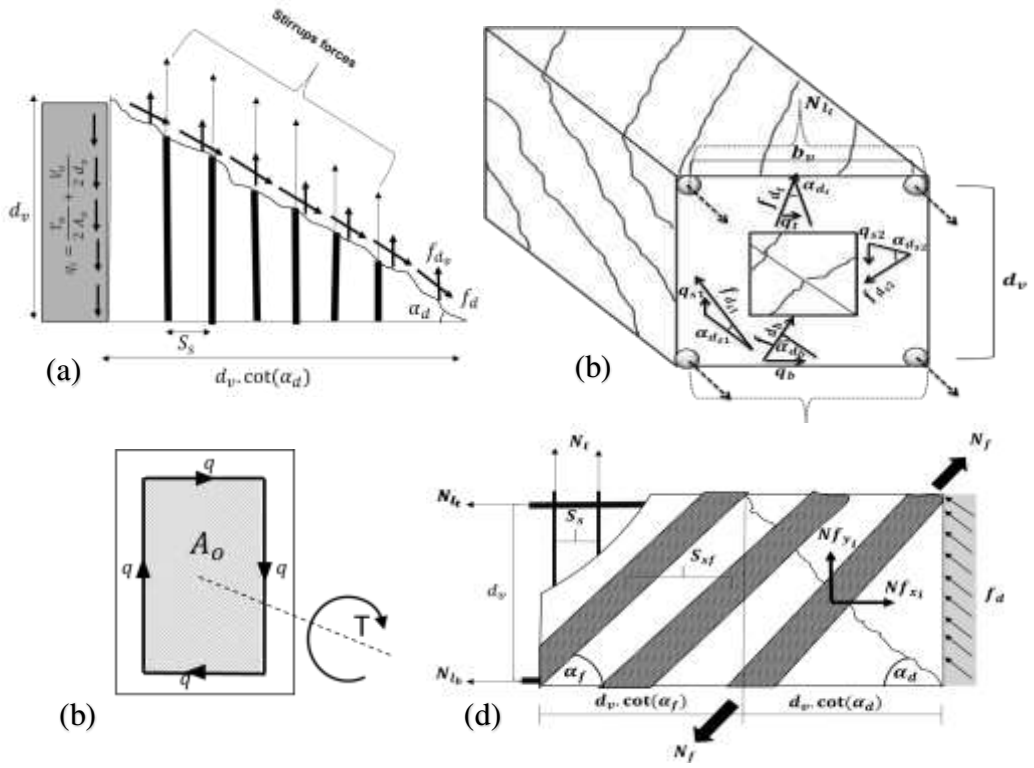


Figure 8. (a) Truss mechanism at the side wall, (b) Space truss mechanism, (c) shear flow and the section's effective area, (d) Truss mechanism for inclined fibres.

The amount of shear flow ($q_i$) and the concrete strut angle ($\alpha_{d_i}$) of each side (wall) of the sections vary, as given in Eq. 5-8 to 5-11. These variations depend on the direction of the torsional and vertical shear forces. For simplicity, a uniform shear distribution has been assumed over the beams' side depths, similar to what was adopted by Greene Jr and Belarbi (2009). The relationship between the inclination angle, the shear flow, and the transverse reinforcement forces is depicted in Figure 8-a. In this figure, the shear flow that is induced by the torque is evaluated according to Bredt's equation (Eq. 5-11). The magnitude of tensile forces in the bottom chords ($N_{l_b}$) for the unstrengthened members can be predicted using Eq. 5-12, which is a rearrangement of Eq. 5-7 (formed by substituting Eq. 5-8 to 5-11).

$$M_u = A_{l_b}F_l(d_V) - 0.5q_{s1}(d_V)\cot(\alpha_{d_{s1}})(d_V) - 0.5q_{s2}(d_V)\cot(\alpha_{d_{s2}})(d_V) - q_b(b_V)\cot(\alpha_{d_b})(d_V) \quad (5\text{-}7)$$

$$\cot(\alpha_{d_i}) = \frac{q_i\, S_s}{A_{t_s} f_{t_y}} \quad (5\text{-}8)$$

$$q_{s1} = \left(\frac{T_u}{2\,A_*} + \frac{V_u}{2\,d_v}\right) \quad (5\text{-}9)$$

$$q_{s2} = \left(\frac{T_u}{2\,A_*} - \frac{V_u}{2\,d_v}\right) \quad (5\text{-}10)$$

$$q_t = q_b = \left(\frac{T_u}{2\,A_*}\right) \quad (5\text{-}11)$$

$$N_{l_b} = \frac{M_u}{dv} + 0.5\left(\frac{T_u}{2\,A_*} + \frac{V_u}{2\,d_v}\right)^2 \left(\frac{d_v\,S_s}{A_{t_s} f_{t_y}}\right) + 0.5\left(\frac{T_u}{2\,A_*} - \frac{V_u}{2\,d_v}\right)^2 \left(\frac{d_v\,S_s}{A_{t_s} f_{t_y}}\right) + \left(\frac{T_u}{2A_*}\right)^2 \left(\frac{b_v S_s}{A_{t_s} f_{t_y}}\right) \quad (5\text{-}12)$$

The evaluation of tensile forces in the main rebars for the strengthened members with vertically oriented wraps needs to consider the influence of the fibre wraps on the inclination angles of the concrete struts of the beam's four sides (left, top, right, and bottom). This can be achieved by accounting for the contribution of the CFRP layer in the vertical direction, as given in Eq. 5-13; where the evaluated angles of inclinations based on Eq. 5-13 should not be more than that obtained from Eq.5-8. Otherwise, the inclination angle is controlled by the yielding of the steel reinforcement before the rupture of CFRP. Following the same steps that were used to develop Eq. 5-12, Eq. 5-14 is introduced to compute the peak tensile forces in the main steel rebars under the combined actions. Similarly, the CFRP contribution can be adopted for the inclined configuration. However, the relationship between the angle fibre strips and concrete struts (which is illustrated in Figure 8-d) has to be determined by establishing force equilibrium in the vertical direction for all sides, as given in Eq. 5-15. Eq. 5-16 is then derived to compute the tensile forces in the inclined CFRP strips along the horizontal direction, where the resultants of these forces are considered at the middle of each wall of the section. Again, rearranging and substituting Eq. 5-15 and Eq.5-16 in Eq. 5-7 produces Eq. 5-17, which allows the computation of the tensile force in the main rebars, with different orientations of fibres.

The proposed formulas can be modified to account for the different directions of flexural forces (e.g. negative bending moment), which would induce the yielding of the upper chords. This can be simply performed by equating the applied bending moment to the internal resisting moment at the bottom side and by following the same procedure to compute the angles of inclinations, shear flow, and rebar forces.

$$\cot(\alpha_{d_i}) = q_i \left(\frac{S_{sf}}{A_f\,E_f\,\varepsilon_{ef}}\right) \quad (5\text{-}13)$$

$$N_{l_b} = \frac{M_u}{d_v} + 0.5\,q_{s1} d_v \cot(\alpha_{s1}) + 0.5\,q_{s2}\,d_v \cot(\alpha_{s2}) + q_b\,b_v \cot(\alpha_b) \quad (5\text{-}14)$$

$$\cot(\alpha_{d_i}) = \frac{q_i\,S_{sf}}{Af\,Ef\,\varepsilon_{ef}\sin(\alpha_f)} - cot(\alpha_f) \quad (5\text{-}15)$$

$$Nf_{xi} = \left(A_f \varepsilon_{ef}\,E_f\,d_v\,S_{sf}{}^{-1}\right) cos(\alpha_f)\left[(cot(\alpha_f) + cot(\alpha_{d_i})\right] \quad (5\text{-}16)$$

$$N_{l_b} = \frac{M_u}{d_v} + 0.5\, q_{s1} d_v \cot(\alpha_{s1}) + 0.5\, q_{s2}\, d_v \cot(\alpha_{s2}) + q_b\, b_v \cot(\alpha_b) - 0.5 \sum_{i=s1}^{i=s2} Nf_{xi} - Nf_{xb} \quad (5\text{-}17)$$

Where $T_u$ is the total torque in N.mm; $q_i$ is the shear flow in N/mm for the section's four sides ($q_{s1}$, $q_{s2}$, $q_t$, and $q_b$); Mu is the maximum applied bending moment in N.mm; $N_{l_b}$ is the tensile force in the bottom chords in N; $A_{l_b}$ is the area of the bottom chords in mm$^2$; $F_l$ is the stress in the bottom chords in MPa; $\alpha_{d_i}$ is the inclination angle of concrete struts for the section's four sides ($\alpha_{d_{s1}}$, $\alpha_{d_{s2}}$, $\alpha_{d_t}$ and $\alpha_{d_b}$); Ss is the spacing between transverse reinforcements in mm; $A_{ts}$ is the cross-sectional area of transverse reinforcements in mm$^2$; $F_t$ is the tensile strength in transverse reinforcements in MPa; $A_f$ is the area of fibres sheet in mm$^2$; $Nf_{xi}$ is the tensile force in the inclined fibres in longitudinal direction for the section's four sides in N; $N_t$ is the tensile force of transverse reinforcements in N; $N_{l_t}$is tensile force in the top chords in N.

# 6 Analytical models of beam-column joints

It is essential to recognise both the shear transfer mechanism of the forces that develop at the joint boundaries and which failures of the RC beam-column connections resulted from inadequate shear strength. Considering the complications involved in the shear mechanism and the influencing parameters that affect the joint's behaviour, a number of empirical and semi-empirical models have been developed to estimate the strength of the joint. Also, several theoretical models have been developed that are derived from the strut-tie theory. These include the fixed angle softened strut-and-tie model (Hwang and Lee, 1999), the modified rotated angle strut-and-tie model (Wong, 2005), the general multi-strut-and-tie model (Pantelides et al., 2002), and the generalized monotonic strut-and-tie model (Parker, 1997). In general, these models mainly require the node dimensions of the struts to be defined; these correspond to the compression zone depths for the beams and columns at the joint boundaries. These models are intended to be applicable to beam-column joints under flexural and axial loads. Alternatively, the panel truss mechanism (compression strut fields-tension ties) for the joint load transfer has been identified by Paulay et al. (1978) and adopted by NZS 3101 (2006). Based on the panel truss mechanism, the Panel Zone Principal Stress-Strain Model was introduced by Pantazopoulou and Bonacci (1992). This model satisfies the equilibrium of forces, compatibly of strain, and the materials' constitutive law. Further, Tsonos (2008), Tsonos (1996),

and Paulay et al. (1978) developed joint models by considering the panel mechanism and direct strut action. These theoretical models have been verified against concentrically loaded members.

In contrast, this study aims to utilise the concepts of the average stress-strain distributions according to the panel zone principal stress-strain method that was developed by (Pantazopoulou and Bonacci, 1992), to predict the joint strength and distortion level when subjected to the set of combined forces . This study re-derives and modifies the panel zone principal stress-strain formulas (Pantazopoulou and Bonacci, 1992) using an iterative approach to satisfy 1) the equilibrium conditions which correspond to the panel truss and the diagonal strut mechanisms proposed by (Tsonos, 2008; Tsonos, 1996; Paulay et al., 1978), 2) the rotating angle theory and 3) the compatibility conditions according to Mohr's circle. Also, this proposed iterative model accounts for the softening of concrete according to an established constitutive model (Belarbi and Hsu, 1995). This approach will also allow the joint distortion to be determined in combination with the joint shear demands; it has been adopted as a more traditional direct strut method, which is based mainly on the equilibrium conditions of the stresses. This means that the strain compatibility, material constitutive conditions, node forces, along with their dimensions, are generally extremely complicated to define under the intricate loading conditions based on the direct strut method found in this investigation.

Based on the concept of average stresses proposed by Pantazopoulou and Bonacci (1992), the distribution of normal stress and shear stress are considered uniform across the joint. The stresses along the main bars of the beam and top face of the joint are illustrated Figure 9-a, where a significant proportion of the beam stresses were introduced into the joint by bond stresses (equal and opposite to the rebar forces $fsl_i$- see Figure 9-c) between the bars and the surrounding concrete. This study assumed that sufficient bonding and anchorage conditions (to maintain the panel mechanism through the diagonal concrete struts) were developed between cracks (Figure 9-c). The kinematics of the joint panel due to the beam shear demand is illustrated in Figure 9-b, which shows the total deformation of the joint as defined by the average angle of distortion ($\gamma$) and longitudinal ($\epsilon_l$) and transverse ($\epsilon_t$) strains. According to the concept of average stresses, the normal vertical compressive stress and shear stress are uniformly distributed over the section's depth.

Referring to Figure 9-c, the equilibrium of forces in the horizontal (l) and transverse (t) directions are given in Eq. 6-1 and 6-2, respectively. The total forces acting in the joint core

correspond to the panel truss; the diagonal strut mechanisms are equated to the joint shear forces ($V_{jh}$ and $V_{jv}$) (Tsonos, 2008; Tsonos, 1996; Paulay et al., 1978), where the force components ($fcl_i$ and $fct_i$) of the concrete strut ($fcD_i$) are added to the truss model forces ( e.g. $fsl_i$ and $fst_i$ ) in the horizontal and vertical direction; these forces equate to the shear demands ($V_{jh}$ and $V_{jv}$) in the same direction. The vertical shear forces can be evaluated according to Eq. 6-3 and Eq.6-4 (Paulay et al., 1978). Eq. 6-5 and 6-6 restate the equilibrium of forces to comply with the average stresses of the two orthogonal directions ($\sigma_l$ and $\sigma_t$); as the average stresses in concrete are equivalent to the average of the developed forces in concrete divided by the joint's area (e.g. $\sigma_{cl} = \frac{\sum_{i=1}^{n} fcl_i}{b_j h_c}$). While the average stresses that developed in the embedded steel rebars ($\sigma_{sl}$ *and* $\sigma_{st}$) ~~in concrete~~ need to be adjusted based on the smeared stress concept (continuous materials, i.e. the stress-strain relationship correctly attained) by multiplying $\sigma_{sl}$ *and* $\sigma_{st}$ by the reinforcement ratios in both the longitudinal and transverse direction of the joint .

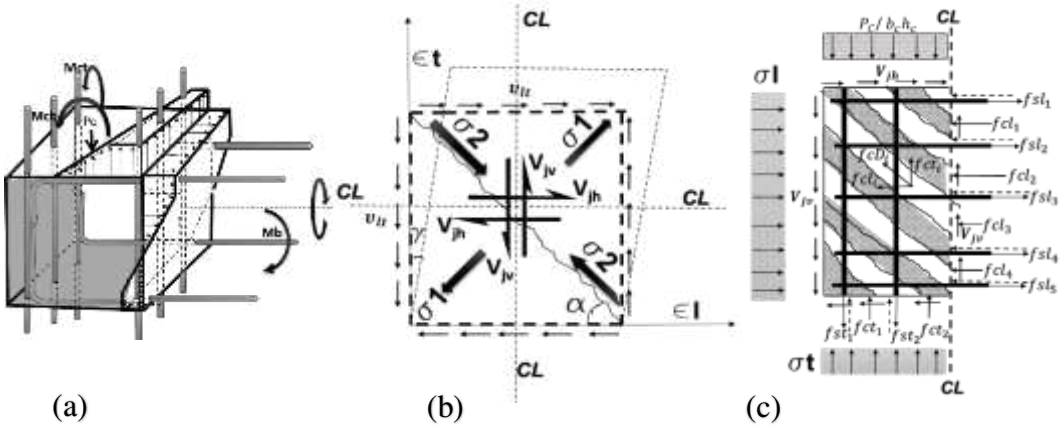


**Figure 9.** (a) Stress variation along steel bars, (b) kinematics of the joints, (c) forces and average stresses in the joint's section.

$$\sum_{i=1}^{n} fcl_i + \sum_{i=1}^{n} fsl_i = V_{jh} \quad (6\text{-}1)$$

$$\sum_{i=1}^{n} fct_i + \sum_{i=1}^{n} fst_i = V_{jv} - P_c \quad (6\text{-}2)$$

$$V_{jv} = \beta V_{jh} \quad (6\text{-}3)$$

$$\beta = \frac{h_b}{h_c} \quad (6\text{-}4)$$

$$\sigma_{cl} + \rho_{sl}\,\sigma_{sl} = v_{lt} \quad (6\text{-}5)$$

$$\sigma_{ct} + \rho_{st}\,\sigma_{st} = v_{lt} - \frac{P_c}{b_c h_c} \quad (6\text{-}6)$$

$$v_{lt} = \frac{V_{jh}}{b_j h_c} \quad (6\text{-}7)$$

Where, $fsl_i$ and $fst_i$ are the forces in the longitudinal and transverse reinforcements, respectively in N; $fcl_i$ and $fct_i$ are the forces in the concrete strut in the longitudinal and transverse directions, respectively in N; $P_c$ is the axial compressive force (column's load) in N; $\sigma_{sl}$ and $\sigma_{st}$ are the stresses in the longitudinal and transverse reinforcement, respectively in MPa; $\sigma_{cl}$ and $\sigma_{ct}$ are the stresses in the concrete in the longitudinal and transverse directions, respectively MPa; $\rho_{sl}$ and $\rho_{st}$ are the reinforcement ratio in the longitudinal and transverse directions, respectively; $\upsilon_{lt}$ is the joint shear stress in MPa; $h_c$ is the column depth in mm; $b_j$ is the joint depth (mm) and $h_b$ is the beam depth in mm.

To evaluate the angle of inclination ($\alpha$) of the concrete strut, the rotating angle theory is employed, where the angle coincides with the principal stresses $\sigma_2 - \sigma_1$ as shown in Figure 9-b. The general transformation matrix for the in-plane stresses in the orthogonal directions (*l-t*) and the principal stress coordinates (1-2) for the concrete is given in Eq. 6-8. Eq. 6-9 to 6-11 are the equilibrium equations, which are compatible with the Mohr truss model. An additional equation that associates the maximum principal stresses of the concrete with the normal stresses along the l and t directions is also required and is given as Eq. 6-12. For simplicity, the principle stress of concrete ($\sigma_1$) is considered to be negligible and, in any plane, the normal stresses are not considered to exceed the concrete compressive capacity.

$$\begin{bmatrix} \sigma_l - \rho_{sl}\,\sigma_{sl} \\ \sigma_t - \rho_{st}\,\sigma_{st} \\ \upsilon_{lt} \end{bmatrix} = \begin{bmatrix} sin_\alpha^2 & cos_\alpha^2 & -2sin_\alpha\, cos_\alpha \\ cos_\alpha^2 & sin_\alpha^2 & 2sin_\alpha\, cos_\alpha \\ sin_\alpha\, cos_\alpha & -sin_\alpha\, cos_\alpha & (cos_\alpha^2 - sin_\alpha^2) \end{bmatrix} \begin{bmatrix} \sigma_1 \\ \sigma_2 \\ 0 \end{bmatrix} \tag{6-8}$$

$$\sigma_2 = -\upsilon_{lt} \frac{1}{sin_\alpha\, cos_\alpha} = -\upsilon_{lt} \left( \frac{1}{tan_\alpha} + tan_\alpha \right) \tag{6-9}$$

$$\sigma_l - \rho_{sl}\,\sigma_{sl} = -\upsilon_{lt}\, cot_\alpha \tag{6-10}$$

$$\sigma_t - \rho_{st}\,\sigma_{st} = -\upsilon_{lt} tan_\alpha \tag{6-11}$$

$$\sigma_2 + \sigma_1 = \sigma_l + \sigma_t \tag{6-12}$$

Three compatibility equations based on Mohr's circle of strain that were reported by Vecchio and Collins (1986) have been used. The relationship between the strain components ($\epsilon_l$ , $\epsilon_t$, $\epsilon_1$, $\epsilon_2$ , and $\gamma_{lt}$) are given by Eq. 6-13 to 6-15. The inclination of the joint's concrete compressive strut (Eq.6-15) can be determined according to the compression stress field theory (Vecchio and Collins, 1986). Finally, the reinforcement is assumed to be adequately anchored within the concrete

such that strain compatibility exists between the two components. Thus, two constitutive equations (Eq.6-16 and 6-17), which conform to Hook's law and neglect the tension stiffening of concrete, are used to evaluate the longitudinal and transverse strains in the bars.

$$\epsilon_2 + \epsilon_1 = \epsilon_l + \epsilon_t \tag{6-13}$$

$$\frac{\gamma_{lt}}{2} = \frac{(\epsilon_1 - \epsilon_l)}{tan_\alpha} \tag{6-14}$$

$$tan_\alpha^2 = \frac{\epsilon_l + \epsilon_2}{\epsilon_t + \epsilon_2} \tag{6-15}$$

$$\epsilon_l = \frac{\rho_{sl}\,\sigma_{sl}}{E_{sl}} \tag{6-16}$$

$$\epsilon_t = \frac{\rho_{st}\,\sigma_{st}}{E_{st}} \tag{6-17}$$

Where $\epsilon_l$ and $\epsilon_t$ are the average strains in longitudinal and transverse directions, respectively; $\epsilon_1$ and $\epsilon_2$ are the average strains in the principal directions, respectively; $E_{sl}$ and $E_{st}$ are the modulus of elasticity for the longitudinal and transverse reinforcement, respectively; $\gamma_{lt}$ is the shear distortion angle.

Referring to the previous equations and relationships between the stresses and strains in the concrete and the reinforcement, the sum of Eq. 6-5, 6-6, 6-10 and 6-11 produce equations (6-18) and (6-19) which allow the evaluation of ($\epsilon_l$) and ($\epsilon_t$) before the initiation of yielding in the joint rebars occur. According to Eq. 6-15, the magnitudes of the principal strains ($\epsilon_1$) and ($\epsilon_2$) are related to the angle of inclination as given in Eq. 6-20 and 6-21. The nominal angle of the inclination of the concrete strut before yielding of the steel ties is computed by associating the maximum compressive strain ($\epsilon_2$) to ($\sigma_2/E_c$) in Eq. 6-15, where $\sigma_2$ is given in Eq. 6-9 and $E_c$ is the modulus of elasticity of concrete. This produces a quadratic polynomial equation (Eq. 6-22) in terms of ($tan_\alpha$).

$$\epsilon_l = \upsilon_{lt}\frac{(cot_\alpha + 1)}{E_{sl}\,\rho_{sl}} \tag{6-18}$$

$$\epsilon_t = \frac{\frac{-P_c}{b_c h_c} + \upsilon_{lt}\beta(1 + tan_\alpha)}{E_{st}\,\rho_{st}} \tag{6-19}$$

$$\epsilon_1 = \frac{(\epsilon_l\, tan_\alpha^2 - \epsilon_t)}{(tan_\alpha^2 - 1)} \tag{6-20}$$

$$\epsilon_2 = \frac{(\epsilon_l - tan_\alpha^2)}{(1 - tan_\alpha^2)} \tag{6-21}$$

$$\left(\frac{\upsilon_{lt}}{E_c} + \frac{\upsilon_{lt}}{E_{sl}\,\rho_{sl}}\right) + \upsilon_{lt}\frac{\tan_\alpha}{E_{sl}\,\rho_{sl}} - \frac{tan_\alpha^3}{E_{st}\,\rho_{st}}\left(\beta\upsilon_{lt} - \frac{P_c}{b_c h_c}\right) - tan_\alpha^4\left(\frac{\beta\upsilon_{lt}}{E_{st}\,\rho_{st}} + \frac{\upsilon_{lt}}{E_c}\right) = 0 \tag{6-22}$$

A rapid decrease in the joint's strength after the yielding of the shear joint's ties occurred was reported by Bonacci and Pantazoupoulou (1993). Thus, when $\epsilon_l$ was equal to ($\frac{\sigma_{sly}}{Esl}$), the angle of inclination is calculated from Eq. 6-23. The vertical strain ($\epsilon_t$) of the reinforcement (ties) is related to the yielding of the horizontal ties by the substitution of Eq. 6-23 in Eq.6-19, as given in Eq. 6-24. Finally, after the yielding of the steel ties, the horizontal and vertical strain ($\epsilon_l \; and \; \epsilon_t$) in equations 6-20 and 6-21 should be replaced by $\epsilon_{ly} \; and \; \epsilon_{ty}$.

$$cot_\alpha = \frac{\sigma_{sly}\,\rho_{sl} - \upsilon_{lt}}{\upsilon_{lt}} \tag{6-23}$$

$$\epsilon_t = \frac{1}{E_{st}\,\rho_{st}}\left(\frac{-P_c\,\sigma_{sly}\,\rho_{sl} + P_c\upsilon_{lt} + b_j h_c \beta \upsilon_{lt}\,\sigma_{sly}\,\rho_{sl}}{\left(\sigma_{sly}\,\rho_{sl} - \upsilon_{lt}\right)}\right) \tag{6-24}$$

The capacity of the compression inclined cracked concrete strut is reduced in accordance with the increase in the tensile strain ($\epsilon_1$). The softening of concrete in compression has been evaluated by Vecchio and Collins (1993), and Belarbi and Hsu (1995). A softened stress-strain relationship is presented in Eq. 6-25 to 6-26; this study utilises the Hsu and Belarbi model to investigate the concrete strut capacity in accordance with the joint's major strains ($\epsilon_l \; and \; \epsilon_t$).

$$\sigma_2 = \xi_{\sigma 0} fc' \left[2\left(\frac{\epsilon_2}{\xi_{\epsilon 0}\epsilon_o}\right) - \left(\frac{\epsilon_2}{\xi_{\epsilon 0}\epsilon_o}\right)^2\right] \tag{6-25}$$

$$\xi_{\sigma 0} = \frac{0.9}{\sqrt{1+400\epsilon_1}} \text{ and } \xi_{\epsilon 0} = \frac{1}{\sqrt{1+500\epsilon_1}} \tag{6-26a}$$

$$f_{max} = \xi_{\sigma 0} fc' \tag{6-26b}$$

Where $\epsilon_o$ is the compression strain at the maximum stress in a uniaxial stress-strain curve for the concrete cylinder, taken as 0.002; $\sigma^o$ is the maximum compression stress in the concrete cylinder in MPa and $\xi$ is the softening coefficient.

To solve the set of equations presented in Section 6, a flow coded program was developed using MATLAB programme. The solution flow chart is illustrated in Appendix I; an iterative method was used to check the concrete strut capacity and the yielding of the bars by incrementing the joint shear ($\upsilon_{lt}$). The joint shear increment is limited to the shear demand, which was calculated in Section 5 of this study.

## 7 Model Validation and Discussion

The peak tensile stresses in the beam's bottom steel for all specimens (SH-U-C, SH-S-C-A, SH-S-C-I, and SH-S-C-H) were calculated according to the equations presented in Section 5 and then compared to the tests results (see Figure 10). Figure 10-a shows good agreement between the

predicted and experimentally obtained results, with a mean value of 0.98 for the ratio of the test to the model results and a corresponding coefficient of variation (COV) of 2%. Table 4 illustrates the predicted ultimate torsional capacity for the tested specimens, along with the computed concrete inclination angle ($\alpha_d$) at the beam's sides and the designed strut concrete capacities ($\sigma_d$), according to Section 5. The given ( $\sigma_{d_v}$) is based on the lowest obtained value at the beam side 1, where torsion and shear act in the same direction (additive). Based on the evaluated percentage differences (Table 4), there was no crushing of concrete before the specimens reached their designed capacities. In addition, the predictions of the strengthened member's behaviour closely followed the actual development of the design load to maximum, and then beyond, as it deteriorated following the peak load. The differences between the analytically and experimentally obtained torsional peak loads are shown in Figure 10-b. This study has taken the partial factors of safety equal to unity for comparative purposes. However, the incorporation of the material safety factors for concrete and CFRP composites are recommended in the relevant design codes, (Eurocode 2, 2004; FIB Bulletin 14, 2001).

The shear distortion angle of the joint zone for each specimen was evaluated according to Eq. 6-14. The comparison between the model and the tests in terms of angle of distortion is shown in Figure 10-c. In this figure, it can be seen that the model can successfully predict joint deformation when it is subjected to different beam forces (shear demands). However, to verify the adequacy of the model and to predict the ultimate joint capacity (failure loads), the tests results of 5 unstrengthened RC beam-column joints (SP1, SP3, SP4, SP7, and SP8), as reported by Elshafiey et al. (2016) were considered. These five specimens failed in the joint zones under combined loading. A comparison between the predicted results using the model developed in this investigation and the tests results from Elshafiey et al. (2016) in terms of maximum joint force ($V_j$) are shown in Figure 10-d. Again, a good correlation is seen, with a mean value of 98% for the ratio of the experimental to the predicted $V_j$; the COV is equivalent to 4%.

The model developed in this investigation has been formulated to evaluate the influence of an increase in beam load on the joint's integrity, which is mainly caused by additional torsional forces that are proportional with the beams' strengthening schemes. It considers that the beam's forces are essentially transferred into the joint zone by the main steel, while the beam's flexural compressive forces at the joint's boundaries (the beam's compressive stress block) will be less

effective in accordance with the ratio of torque to bending. The magnitude of the main rebar forces corresponds to the level of bending, torsional and shear forces (Eq. 5-12, 5-14 and 5-17) that can be carried by the beam. However, the beam carrying capacity is limited by the concrete strut strength (Eq. 5-6), while the effect of the transverse reinforcement (stirrups and CFRP) are represented in the strut's inclination angle (Eq.5-8, 5-13 and 5-15), in which both components have an effect on the strut and the steel forces (Eq.5-5, 5-12, 5-14, and 5-17).

Similarly, the shear resistance capacity of the joint zone through all the solution stages is limited by the peak strength of the softened concrete (Eq.6-25 to Eq.6-26). The derived expressions in Section 6 account for the effect of the reinforcement ratios ( $\rho_{sl}$ and $\rho_{st}$ ), the column axial load ($P_c$) and the joint aspect ratio (β) on the joint capacity and its distortion level. It was also noticed that the effectiveness of the joint's reinforcement was enhanced by an increase in concrete strength ($f_c'$). These joint expressions could also be adjusted to consider joints that are externally bonded with uniaxially CFRP systems as illustrated in Appendix II.

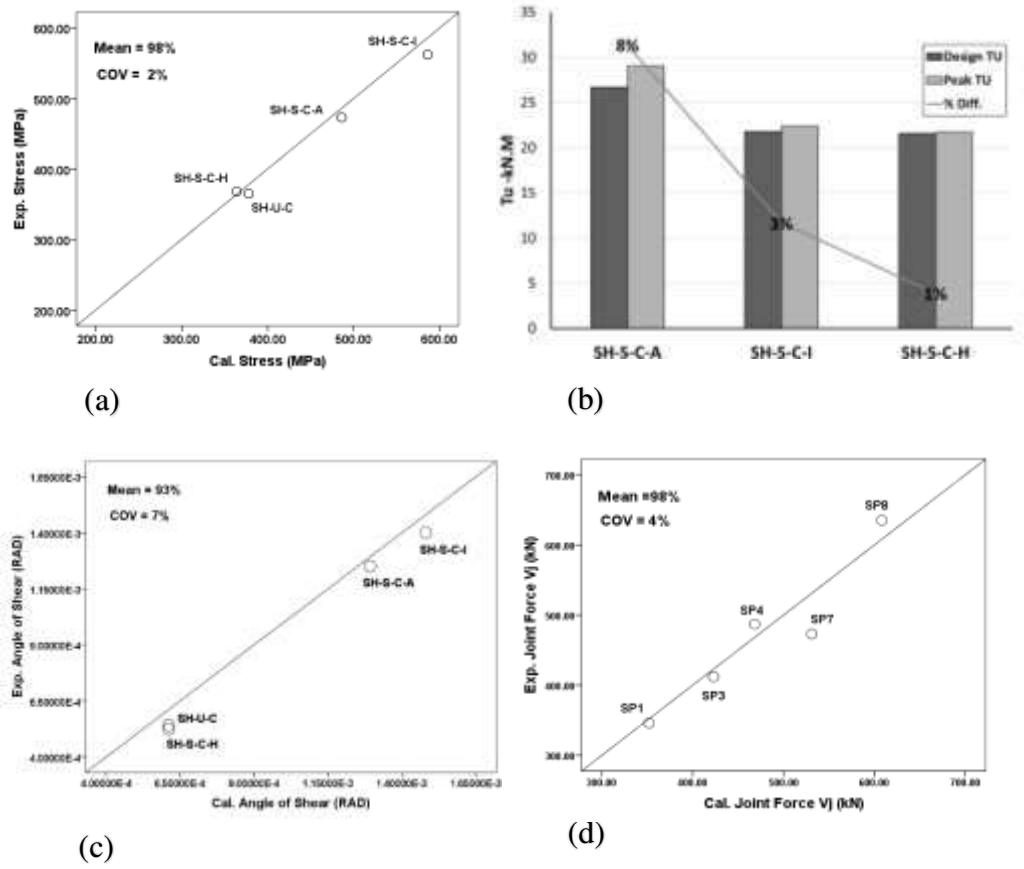


**Figure 10.** Experimental versus predicted results: (a) bottom stinger forces, (b) Design and Peak Tu, (c) Max. Joint distortion angles, (d) Max. joint forces (Vj).

## 8 Conclusions

The behaviour of the four reinforced concrete exterior beam-column joints have been discussed and analysed. In general, the test outcomes demonstrated the influence of beam wrapping (with full and partial CFRP wrapping configurations) on both failure modes and the joint demands. The viability of using CFRP wrapping systems to enhance member carrying capacities under torsional actions was confirmed. The enhancement levels were affected by the fibre ratio, the degree of confinement and the fibre's orientation. Ductility of the members was reduced owing to the degree of concrete strut degradation, which was related to the magnitude of shear stresses produced by the addition of torsion and shear forces and due to the degree of wrapping. To avoid the concrete crushing, this study recommends limiting the reinforcement forces that resulted from the superposition of the CFRP and rebars, such that the capacity of the concrete struts is not exceeded. The strain readings confirmed the influence of the torsional forces; these forces increased the tensile stresses in the beam steel, which affected the shear demand and distortion levels of the joints. It was clear that the joint's shear forces that were transferred into the joint from the beam's reinforcement would be underestimated if they were based only on the bending stresses without any consideration for the torque and shear forces. Apart from for beams loaded in flexure, no code provisions for RC joints exist to quantify the joint shear demands arising from combined beam loading (flexure, torsion, shear).

This study proposes a number of formulas based on the truss mechanism which are intended to be used to quantify the joint forces and which consider the effects of combined loads and different wrapping schemes. It also introduces a design approach which accounts for the level of developed compression forces due to shear-flow levels in order to prevent a concrete failure. Finally, it develops an iterative model, according to the average stress concept, that can be used to predict the joint capacity. This model addresses the softening of the concrete and the truss and inclined stress field mechanisms and has been verified against independent experimental data.

**Acknowledgment:** The authors wish to acknowledge the contribution of the Ministry of Higher Education and Scientific Research of the Republic of Iraq for funding this research project.

## REFERENCES


ACI-ASCE 352R-02 Committee. (2002) Recommendations for design of beam-column joints in monolithic reinforced concrete structures. American Concrete Institute.

ACI Committee 318. (2014) Building code requirements for structural concrete and commentary. American Concrete Institute.

Al-Bayati G, Al-Mahaidi R, Hashemi MJ, et al. (2018) Torsional strengthening of RC beams using NSM CFRP rope and innovative adhesives. *Composite Structures* 187: 190-202.

Ali S and Forth J. (2018) Behaviour of torsionally strengthened reinforced concrete beam-column joints with carbon fibre reinforced polymer dheets. *Proceedings of The 12th fib International PhD Symposium in Civil Engineering*.

Allawi AA, Chai HK and Majeed AA. (2015) Torsional Analysis of Multicell Concrete Box Girders Strengthened with CFRP Using a Modified Softened Truss Model. *Journal of Bridge Engineering* 20: B4014001.

Ameli M, Ronagh HR and Dux PF. (2007) Behavior of FRP Strengthened Reinforced Concrete Beams under Torsion. *Journal of Composites for Construction* 11: 192-200.

Antonopoulos CP and Triantafillou TC. (2003) Experimental Investigation of FRP-Strengthened RC Beam-Column Joints. *Journal of Composites for Construction* 7: 39-49.

Atta AM and El-Shafiey TF. (2014) Strengthening of RC dapped-end beams under torsional moment. *Magazine of Concrete Research* 66: 1065-1072.

Belarbi A and Hsu TT. (1995) Constitutive laws of softened concrete in biaxial tension compression. *Structural Journal* 92: 562-573.

Bonacci J and Pantazoupoulou S. (1993) Parametric Investigation of Joint Mechanics. *Structural Journal* 90.

BS8110. (1997) Structural Use of Concrete, Part 1: Code of Practice for Design and Construction. *British Standards Institution, UK*.

CEB-FIP C. (1991) model code 1990. *Comite Euro-International Du Beton, Paris*: 87-109.

Chalioris CE. (2008) Torsional strengthening of rectangular and flanged beams using carbon fibre-reinforced-polymers – Experimental study. *Construction and Building Materials* 22: 21-29.

Chun S-C and Shin Y-S. (2014) Cyclic Testing of Exterior Beam-Column Joints with Varying Joint Aspect Ratio. *ACI Structural Journal* 111: 693.

Davood M and Alireza A. (2017) Flexural Strengthening of Reinforced Concrete Beam-Column Joints Using Innovative Anchorage System. *ACI Structural Journal* 114.

Deifalla A, Awad A and Elgarhy M. (2013) Effectiveness of externally bonded CFRP strips for strengthening flanged beams under torsion: An experimental study. *Engineering Structures* 56: 2065-2075.

Deifalla A and Ghobarah A. (2010) Strengthening RC T-Beams Subjected to Combined Torsion and Shear Using FRP Fabrics: Experimental Study. *Journal of Composites for Construction* 14: 301-311.

Elfgren L. (1972) Reinforced concrete beams loaded in combined torsion, bending and shear: a study of the ultimate load-carrying capacity. Division of Concrete Structures, Chalmers University of Technology.

Elshafiey TM, Atta AM, Afefy HM, et al. (2016) Structural performance of reinforced concrete exterior beam–column joint subjected to combined shear and torsion. *Advances in Structural Engineering* 19: 327-340.

Eurocode 1. (2002) Actions on structures-Part 1-1: General actions-Densities, self-weight, imposed loads for buildings.

Eurocode 2 B. (2004) 1-2: 2004 Eurocode 2: Design of concrete structures-Part 1-2: General rules-Structural fire design. *European Standards, London*.

FIB Bulletin 14. (2001) *Externally bonded FRP reinforcement for RC structures,* Lausanne, Switzerland.: fib - International Federation for Structural Concrete.

FIB Model Code (Fédération Internationale du Béton). (2010) final draft,. *Bulletin 66* vol.2.

Ghobarah A, Chidiac SE and Ghorbel MN. (2002) Upgrading Torsional Resistance of Reinforced Concrete Beams Using Fiber-Reinforced Polymer. *Journal of Composites for Construction* 6: 257-263.

Greene Jr G and Belarbi A. (2009) Model for Reinforced Concrete Members under Torsion, Bending, and Shear. I: Theory. *Journal of Engineering Mechanics* 135: 961-969.

Hamil SJ. (2000) Reinforced concrete beam-column connection behaviour (BL). ProQuest Dissertations Publishing

Hassan WM. (2011) Analytical and Experimental Assessment of Seismic Vulnerability of Beam-Column Joints without Transverse Reinforcement in Concrete Buildings. ProQuest Dissertations Publishing.

Hii A and Al-Mahaidi R. (2004) Torsional strengthening of reinforced concrete beams using CFRP composites. *Proceedings 2nd international conference on FRP composites in civil engineering, Adelaide, Australia. Balkema, London.* 551-559.

Hii AKY and Al-Mahaidi R. (2007) Torsional Capacity of CFRP Strengthened Reinforced Concrete Beams. *Journal of Composites for Construction* 11: 71-80.

Hsu TT. (1996) Toward a unified nomenclature for reinforced-concrete theory. *Journal of Structural Engineering* 122: 275-283.

Hwang S-J and Lee H-J. (1999) Analytical Model for Predicting Shear Strengths of Exterior Reinforced Concrete Beam-Column Joints for Sesimic Resistance. *ACI Structural Journal* 96: 846-857.

Kusuhara F, Azukawa K, Shiohara H, et al. (2004) Tests of reinforced concrete interior beam-column joint subassemblage with eccentric beams. *13th World Conference on Earthquake Engineering, Vancouver, BC, Canada.*

Ma S, Bunnori NM and Choong KK. (2018) Prediction of Ultimate Torque of Reinforced Concrete Box Beam Bonded with CFRP Strips. *KSCE Journal of Civil Engineering* 22: 4353-4363.

Mohammadizadeh M and Fadaee M. (2010) Experimental and analytical study on behaviour of CFRP-strengthened HSC beams with minimum reinforcement under pure torsion. *Iranian Journal of Science and Technology* 34: 35.

Mostofinejad D, Akhlaghi A and Eslami A. (2018) Estimating the Seismic Performance of CFRP-Retrofitted RC Beam-Column Connections Using Fiber-Section Analysis. *Journal of Earthquake Engineering* 22: 1092-1110.

Mostofinejad D and Hajrasouliha M. (2019) 3D beam--column corner joints retrofitted with X-shaped FRP sheets attached via the EBROG technique.(Report). *Engineering Structures* 183: 987.

NZS 3101. (2006) Concrete structure standard-the design of concrete structures incorporating amendment No. 1 & 2 (NZS 3101: Part 1: 2006-A1&A2). SNZ Wellington, New Zealand.

Panchacharam S and Belarbi A. (2002) Torsional behavior of reinforced concrete beams strengthened with FRP composites. *First FIB Congress, Osaka, Japan.* 01-110.

Pantazopoulou S and Bonacci J. (1992) Consideration of questions about beam-column joints. *ACI Structural Journal* 89: 27-36.

Pantelides CP, Hansen J, Nadauld J, et al. (2002) Assessment of reinforced concrete building exterior joints with substandard details. *PEER report* 18.

Parker DE. (1997) Shear strength within reinforced concrete beam-column joints. ProQuest Dissertations Publishing

Parvin A, Altay S, Yalcin C, et al. (2010) CFRP Rehabilitation of Concrete Frame Joints with Inadequate Shear and Anchorage Details. *Journal of Composites for Construction* 14: 72-82.

Patel PV, Jariwala VH and Purohit SP. (2016) Torsional Strengthening of RC Beams Using GFRP Composites. *Journal of The Institution of Engineers (India): Series A* 97: 313-322.

Paulay T, Park R and Preistley M. (1978) Reinforced concrete beam-column joints under seismic actions. *Journal Proceedings.* 585-593.

Peng X-N and Wong Y-L. (2011) Experimental study on reinforced concrete walls under combined flexure, shear and torsion. *Magazine of Concrete Research* 63: 459-471.

Rabbat BG and Collins MP. (1978) A variable angle space truss model for structural concrete members subjected to complex loading. *Special Publication* 55: 547-588.

Raffaelle G, Gentry T and Wight J. (1992) Earthquake loading on R/C beam-column connections. *10th World Conference on Earthquake Engineering, Balkema, Rotterdam.* 3185-3190.

Salom PR, Gergely J and Young DT. (2004) Torsional Strengthening of Spandrel Beams with Fiber-Reinforced Polymer Laminates. *Journal of Composites for Construction* 8: 157-162.

Sarsam K and Phipps M. (1985) The shear design of in situ reinforced concrete beam–column joints subjected to monotonic loading. *Magazine of Concrete Research* 37: 16-28.

Sasmal S. (2009) Performance evaluation and strengthening of deficient beam-column sub-assemblages under cyclic loading. University of Stuttgart.

Shannag MJ and Alhassan MA. (2005) Seismic Upgrade of Interior Beam-Column Subassemblages with High-Performance Fiber-Reinforced Concrete Jackets. *ACI Structural Journal* 102.

Shigeru Hakuto RP and Hitoshi T. (2000) Seismic Load Tests on Interior and Exterior Beam-Column Joints with Substandard Reinforcing Details. *ACI Structural Journal* 97.

SHIMIZU Y, Zhou J, Hirosawa M, et al. (2000) Effect of the Torsional Moment on the Shear Strength of Reinforced Concrete Due to Eccentric Jointing of beam to column. *World Conference on Earthquake Engineering.* 0859-0851? 0859.

Triantafillou TC and Antonopoulos CP. (2000) Design of Concrete Flexural Members Strengthened in Shear with FRP. *Journal of Composites for Construction* 4: 198-205.

Triantafillou TC and Antonopoulos CP. (2003) Experimental Investigation of FRP-Strengthened RC Beam-Column Joints. *Journal of Composites for Construction* 7: 39-49.

Tsonos A. (1996) Influence of p-delta effect and axial force variations on seismin performance of R/C beam-column joints. *11 th World Conference on Earthquake Engineering.*

Tsonos AG. (2008) Effectiveness of CFRP-jackets and RC-jackets in post-earthquake and pre-earthquake retrofitting of beam–column subassemblages. *Engineering Structures* 30: 777-793.

Vecchio FJ and Collins MP. (1986) The modified compression-field theory for reinforced concrete elements subjected to shear. *ACI J.* 83: 219-231.

Vecchio FJ and Collins MP. (1993) Compression Response of Cracked Reinforced Concrete. *Journal of Structural Engineering* 119: 3590-3610.

Wong HF. (2005) Shear strength and seismic performance of non-seismically designed reinforced concrete beam-column joints.

Zhang J, Lu Z and Zhu H. (2001) Experimental study on the behaviour of RC torsional members externally bonded with CFRP. *FRP Composites in Civil Engineering. Proceedings of the International Conference on FRP composites in Civil Engineering.*